

Nearshore sediment entrainment under breaking waves

Bradley D. Johnson

US Army Engineer Research and Development Center
Coastal and Hydraulics Lab, HC-C
3909 Halls Ferry Road
Vicksburg, MS 39180-6199
johnsob@wes.army.mil

1 Introduction

Hydrodynamic modeling of the nearshore environment has reached some level of maturity over the past several decades. This is primarily because the equations are well defined, and the parts that are not well understood, like the depth dependence of turbulent kinetic energy, play a secondary role in the solution. Modeling sediment transport, on the other hand, has not yet approached a similar level of accuracy. The present tools for predicting shoreline and beach-face change rely on assumptions that simplify the problem and render a tractable computational exercise for an otherwise unwieldy and complex problem. Without a basis in the physical processes of sediment transport, however, these tools rely on site-specific empirical parameters and are only applicable within a narrow range of calibration. Recent improvements in understanding of sediment transport may provide improvements to the morphology models, but the vast separation in modeled time and length scales has not been bridged.

It is commonly accepted that the wind wave induced hydrodynamics are the primary agent for entraining sediment in the nearshore arena. Incident short waves typically have velocities larger than the

currents, and the non-steady nature acts to increase the momentum coupling with the bed. Additional effects due to the breaking process in the surf may also enhance the capacity for wind waves to entrain sand. Phase-resolving models such as those based on the nonlinear shallow-water or Boussinesq equations are capable of predicting the hydrodynamic characteristics on natural beaches [e.g. Raubenheimer *et al.* 1995]. It is therefore reasonable to begin development of modeling technologies that rely on phase-resolving models to predict the entrainment process.

Current and low frequency hydrodynamic modeling is widely embraced for the prediction of setup, undertow, and longshore currents. The phase-averaged hydrodynamic system is the one most frequently used as a foundation for sediment transport models also. Difficulties arise, however, in developing a general sediment transport algorithm within a phase-averaged context, and these attempts have been largely unsuccessful. The details of near-bed hydrodynamics are roughly estimated and poorly represented in the models. As a result, the tools for predicting shoreline and beach-face change rely on assumptions that simplify the problem to render a tractable computational exercise. This limi-

tation makes the present models applicable in simple cases but rely principally on site-specific empirical parameters. The results, understandably, can be in gross error for conditions beyond the calibration range such as severe storm events or for regions without supporting data.

A modeling system embracing both the wave and current model scales is under development that uses process-based high-fidelity model results along with a phase-averaged current model to develop physically-based nearshore morphology predictions. A full description of this coupled model is lengthy, and the focus herein is on the phase-dependent hydrodynamics and sediment entrainment processes.

The present effort outlines an approach for using a one-dimensional nearshore hydrodynamic model together with simple turbulence balances to develop rational estimates of sediment entrainment and wave-related sediment flux. These results represent the first part of a larger effort to develop a process-based nearshore morphology model, but the details of the longer term morphology are beyond the scope of this effort. Model results for hydrodynamics and sediment entrainment are compared with the detailed laboratory data from the Large-scale Sediment Transport Facility (LSTF) at ERDC. Including the surface breaking process in the sediment entrainment function results in improved model predictions when compared with data.

2 Experiment Set-up

A brief description of the Large-scale Sediment Transport Facility (LSTF) is given herein, and the interested reader is referred to the exhaustive report on the design, instrumentation, and capabilities of the tank by Hamilton *et al.* [2000]. The LSTF measures approximately 25 m in the cross-shore by

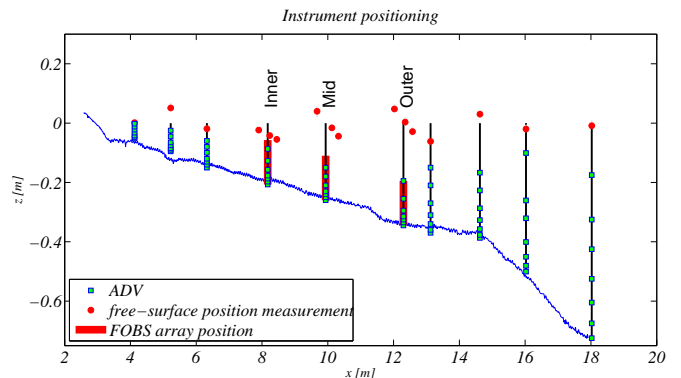


Figure 1: Laboratory instrumentation

30 m alongshore where the walls are angled relative to a cross-shore transect to act as wave guides for the obliquely incident waves. Unidirectional waves were generated with four synchronized paddles rotated to create long crests oriented 10° from the long straight shoreline. A pump system was designed to re-circulate the wave-generated longshore current from the downstream boundary to the upstream boundary of the facility, thus allowing the laboratory basin to function as an infinitely long cylindrical coast. The cross-shore distribution of the longshore current is regulated by 20 independently controlled pumps through 20 channels at the down-drift end of the tank.

The sand beach was part of a larger sediment transport investigation, and was comprised of well-sorted quartz sand with a median grain diameter of 0.15 mm. Figure 1 presents a measured cross-shore bottom profile near the center of the tank showing the ripples. The wave conditions used in this study have been used extensively in other efforts, and the beach profile is based on previously measured profiles that were considered to be in equilibrium. With the exception of the swash zone, bedforms were reasonably uniform in height and length

across the beach. Just seaward of the swash zone, the ripples measured approximately 1 cm in height and 8 cm in length. The height and length of ripples in the mid-surf zone measured 0.7 cm and 7 cm, similar in dimension to the ripples measured in the region immediately seaward of the bar with 0.6 cm and 7 cm. In combined wave and current environments, the ripple orientation can become irregular for sufficiently strong currents. In the portion of the tank that is used for this study, the ripple crests were visually observed to be wave-dominated, meaning that the crests were oriented essentially perpendicular to the wave propagation direction, from $\sim 10^\circ - 5^\circ$ relative to a cross-shore transect.

Synchronized free surface elevation, velocity, and concentration data were collected from a movable instrument bridge spanning a cross-shore transect. Ten capacitance-type surface piercing wave gauges, sampled at 20 Hz, were used to measure the free-surface elevation. Velocity data were collected with ten Acoustic Doppler Velocimeters (ADV) at the same position in the cross-shore and were synchronized with the wave gauges. Suspended sediment concentrations in the LSTF are measured with a single Fiber Optical Back-scatter (FOBS) instrument that was moved to positions through the surf. Each sampling duration was ten minutes long, and complete vertical coverage was accomplished by moving the instrument elevation. Stationarity in the wave field was assured by using the same wave paddle-position time series for each sampling duration. The repeating wave paddle time series can be treated as an ensemble as utilized in the following analysis. Detailed velocity data at ten positions over the water column were compiled for a single cross-shore transect near the center of the tank. The vertical positioning of the measurement locations as well as the cross-shore placement of the instruments is shown in Figure 1.

3 Sediment concentration data

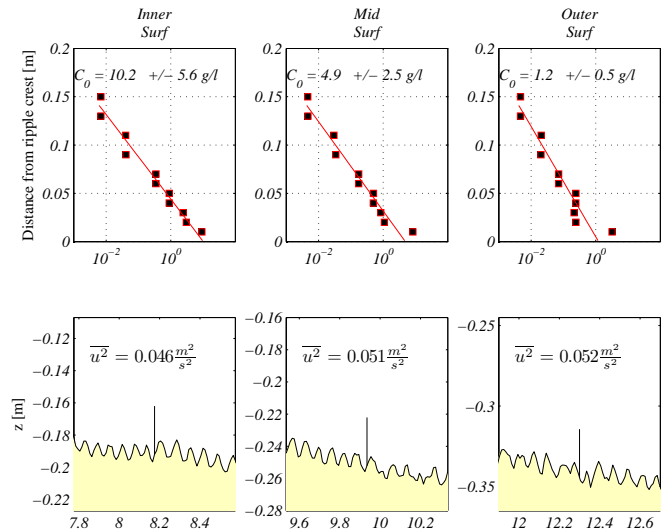


Figure 2: Sediment concentration, bed conditions, and velocity moments at three measurement locations

The complete results and data description of the LSTF CS test are available in Johnson and Smith [2006]. One of the notable results that is pertinent to this discussion, however, is shown in Figure 2. The lower panels show the measured bed ripples at each of the three measurement locations. Also indicated is the time-averaged squared total near-bed velocity $\overline{u^2}$. Considering the similar bedforms and values of $\overline{u^2}$ that differ by less than 10%, it is expected that the time averaged bed shear stress is also similar. Small differences in shear stress through the surf zone can arise from variation in, for instance, a non-constant coefficient of friction with changing wave-Reynolds number or relative bed roughness. However, accounting for these differences does not change the conclusion that the bottom shear stresses are essentially equal at the

three measurement locations [Johnson and Smith 2006]. It is remarkable to note in the upper three panels, then, that the measured near-bed concentrations vary by an order of magnitude over the surf zone as seen in Figure 2. Clearly, the cause and effect relationship typically assumed between the bed shear stress and near-bed concentration is flawed in this shallow, breaking environment.

4 Phase-dependent waves and transport

Phase-resolving nearshore cross-shore models can predict intra-wave surf zone hydrodynamics with impressive accuracy [e.g. Musumeci 2005]. Although the shallow water equations have been used as the basis for some studies including sediment [Kobayashi and Johnson 2001], the Boussinesq equations offer improved dispersion characteristics and more accurate prediction of wave shape. To begin, a general conservation statement is given:

$$\frac{\partial \mathbf{U}}{\partial t} + \frac{\partial \mathbf{F}}{\partial x} = \mathbf{S} \quad (1)$$

with unknown vector \mathbf{U} , fluxes \mathbf{F} , sources \mathbf{S} , cross-shore spatial coordinate x , and time t . To properly model the hydrodynamics for entrainment, a variant of the Boussinesq equations due to Madsen and Sorenson [1992] and extended by Dingemans [1997] is utilized. The phase-dependent equations are solved with a simple predictor corrector method where the Boussinesq terms are included as source terms in the momentum equations. The one-dimensional phase-resolving variables in (1) are

given in conservative form as

$$\begin{aligned} \mathbf{U} &= \begin{bmatrix} h \\ q + \mathbf{b} \\ hC \end{bmatrix} \\ \mathbf{F} &= \begin{bmatrix} q \\ \frac{q^2}{h} + \frac{g}{2}h^2 \\ qC \end{bmatrix} \\ \mathbf{S} &= \begin{bmatrix} 0 \\ -gh\frac{\partial z_b}{\partial x} - \tau_b/\rho + \mathbf{B} \\ S - c_0w_f \end{bmatrix} \end{aligned} \quad (2)$$

where h is the total water depth, q is the volume flux of water, \mathbf{b} represents extra Boussinesq terms as given in Dingemans [1997], C is the depth averaged volumetric concentration of sand in the water column, z_b is the bed position, τ_b is the bed shear stress, \mathbf{B} represents Boussinesq terms as given in Dingemans [1997], S is an entrainment function, c_0 is the near bed concentration, and w_f is the sediment fall velocity.

Figure 3 shows the measured and modeled time series of free surface position at thirteen cross-shore positions to indicate the degree of accuracy in phase speed and wave profile evolution. The top panel is the outer surf zone, the middle panel is in the mid surf zone and the last shows the inner surf. The accurate model to data comparisons allows some confidence in using these hydrodynamic results as forcing for a sediment model.

The depth-integrated sediment conservation statement given in (2) balances the rate of sediment volume change with advection and local entrainment and deposition. Typical bedload and total load formulations use a conventional reference concentration approach for quasi steady flows [e.g. Van Rijn 1984]. The present formulation, however, utilizes the alternate flux boundary bottom boundary condition due to the rapidly varying flows

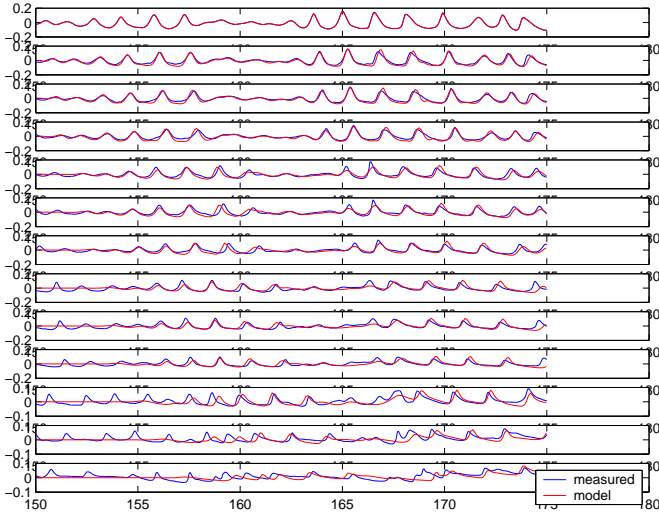


Figure 3: Time-series of free surface position at thirteen cross-shore locations

and the large intra-wave concentration variations expected for this wave-dominated flow. A generalized dissipation based entrainment function following Kobayashi and Johnson [2001] is given as

$$S = \frac{1}{g(s-1)} e\epsilon \quad (3)$$

where e is an empirical efficiency factor and ϵ is a near-bed dissipation.

Sediment transport models typically relate either directly or indirectly to the near bed shear stress or the near-bed turbulence which is assumed to be bed shear generated [see, e.g. Nielsen 1992]. However, data from the shallow and saturated surf zone presented in Figure 2 indicate a significant departure from this idea. Even sophisticated models accounting for wave and current interaction and bed conditions would result in predictions that are similar at the three measurement stations. It is postulated herein that the ten-fold increase in concentration in

the inner surf zone is related to the proximity of the bed to the breaking process. Therefore, a proper prediction of near-bed dissipation ϵ in (3) should include production due to both bottom shear and wave breaking within the nearshore modeling domain. Strictly speaking, the nonlinear nature of turbulence dissipation does not allow for the superposition of dissipation from decoupled analyses of the bed and surface. Bradshaw [1974] and Hunt [1984] have concluded, however, that boundary generated turbulence and externally generated turbulence are statistically independent. On that basis, it is suggested that uncoupled treatments of the two regions along with a linear addition of dissipation is suitably accurate in this analysis.

$$\epsilon = \epsilon_B + \epsilon_f \quad (4)$$

where ϵ_B is dissipation with a wave breaking origin, and ϵ_f is dissipation arising from bottom shear turbulence.

4.1 Breaking turbulence

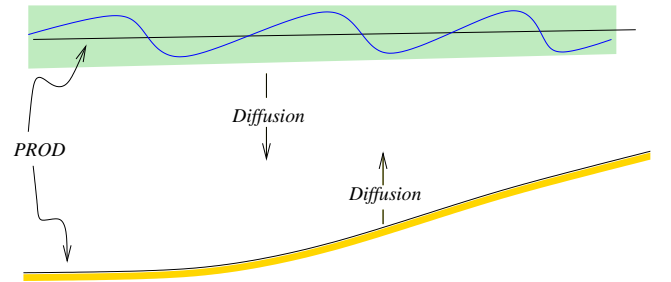


Figure 4: Conceptual description of surf zone turbulence

A simple treatment of surf zone turbulence due to breaking near the surface is developed with the

$k-l$ model:

$$\frac{\partial k}{\partial t} = -\frac{\partial kU}{\partial x} + \frac{\partial}{\partial z} \left\{ \nu_t \frac{\partial k}{\partial z} \right\} + P - \epsilon \quad (5)$$

Where k is the turbulent kinetic energy, U is the depth-averaged horizontal velocity, l_d is prescribed dissipation length scale, $\nu_t = l_d \sqrt{k}$ is the turbulent diffusivity, P is the production of k by wave breaking, and dissipation $\epsilon = c_2 \frac{k^{3/2}}{l_d}$. In keeping with the model outlined in Fredsoe and Deigaard [1992], the dissipation length scale l_d is taken to be $h/10$. A detailed treatment of dissipation based on coupled hydrodynamic and turbulence models would be optimal, but it would be exceedingly complex, computationally intensive, and difficult to justify as a single part of this unproven procedure. Therefore, a strategy for using the robust hydrodynamic model and simple concepts about turbulent balances along with Equation 5 to generate realistic near-bed dissipation rates is presented in the following. A conceptualized view of nearshore turbulence for spilling breakers is offered in Figure 4 where production of turbulence occurs near the surface due to breaking and near the bed due to bottom shear, while diffusion and advection function to distribute. Strictly speaking, of course, this is a gross simplification for sheared flows and the associated production of k throughout the water column. As a first approximation, however, the production of k is assumed to occur in a surface layer and in a bottom boundary layer only. Interestingly, the laboratory measurements of Cox [1995] show horizontal velocities under spilling waves that are nearly depth-uniform, which lends assurance to the simplified turbulence balance. The surface production is computed by a bulk energy balance of the depth-integrated flow for dissipation D :

$$\frac{\partial E}{\partial t} + \frac{\partial E_f}{\partial x} = -D \quad (6)$$

where the energy density E and energy flux E_f are straightforward to derive from the expressions (2) but are beyond the scope of this work [see, e.g. Svendsen 2006]. The hydrodynamic model includes the effect of shear stress, and therefore the computed dissipation is comprised of a bottom shear component as well as a breaking component $D = D_B + D_f$. It is assumed that the breaking-generated production is distributed within the top grid layer with thickness Δz , such that production $P = D/\rho/\Delta z$. With a time-dependent mechanism for the production of k at the surface, the time and spatial variation is readily developed through a numerical integration of (5), and a snapshot of dissipation ϵ distributed over the surf zone is shown in Figure 5. The magnitude of predictions of dissipation rates are very large near the surface production layer and are consistent with the field measurements of George *et al.* [1994] under the trough level. This rudimentary balance shows, also, how surface breaking can extend to the bottom and may play a important role in nearshore entrainment of sediment.

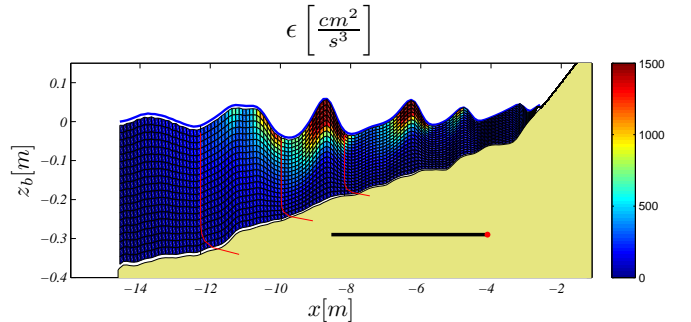


Figure 5: Example of computed instantaneous distribution of dissipation attributed to the breaking-generated turbulence

4.2 Bottom shear turbulence

In keeping with the simple and practical treatment for modeling turbulence due to breaking, the effect of the the bottom boundary layer relies on a rational statement about turbulence production without a detailed analysis. In the thin wave boundary layer, it is assumed that shear-generated production is balanced by dissipation at all times. While the actual distribution of dissipation with distance from the bed is beyond the scope of this effort, but we can expected it to drop off quickly outside of the thin wave boundary layer. Figure 8 shows the approach used in this effort to arrive at a reasonable estimate of ϵ_f without the computational cost associated with a full treatment. The instantaneous dissipation is given with quadratic shear:

$$\epsilon_f = \rho c_f |u|^3 \quad (7)$$

Assuming that the dissipation is negligible in the upper region $z > 2\delta$ where δ is the thickness of the wave boundary layer as presented in Johnson and Smith [2006], then a representative dissipation $\hat{\epsilon}_f$ is developed:

$$\hat{\epsilon}_f = \frac{c_f}{2\delta} |u|^3 \quad (8)$$

With the combined dissipation estimates due to surface breaking and bottom shear, sediment is entrained into the water column according to (3). Through this simple distribution of turbulence due to breaking and bottom shear, the combined dissipation can be treated with one empirical parameter e rather than the two efficiencies that were presented in Kobayashi and Johnson [2001].

4.3 Suspended sediment

The distribution of sediment with depth is assumed to approximate the balance of diffusive upward flux and sediment fall at all times such that

$$c = c_0 e^{\frac{-w_f}{\nu_s} z} \quad (9)$$

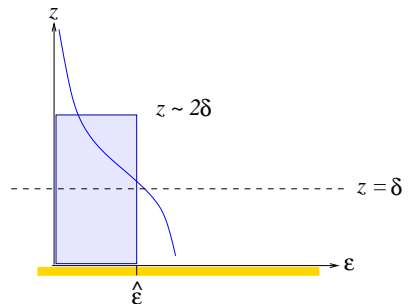


Figure 6: Conceptual description of the dissipation near the bed

where c_0 is the near-bed concentration determined to satisfy the sediment balance in (2):

$$c_0 = \frac{Chw_f}{\nu_t} \left\{ 1 - e^{\frac{-w_f h}{\nu_s}} \right\}^{-1} \quad (10)$$

The sediment diffusivity ν_s in (9) is assumed to be equal to the momentum diffusion expression for breaking waves due to Okayasu [1989]

$$\nu_s \simeq \nu_t = 0.01h\sqrt{gh} \quad (11)$$

Using the measured free-surface data as a boundary condition for the Boussinesq model, the velocity field can be computed used to predict sediment concentrations. The computed time-averaged near bed concentration c_0 based on a simple quadratic bed shear stress alone (without accounting for surface breaking) and the entrainment model Van Rijn [1984] is shown in Figure 7. As expected from the measured results previously presented, the shear stress based on bottom orbital velocities is relatively constant throughout the surf zone. It follows,

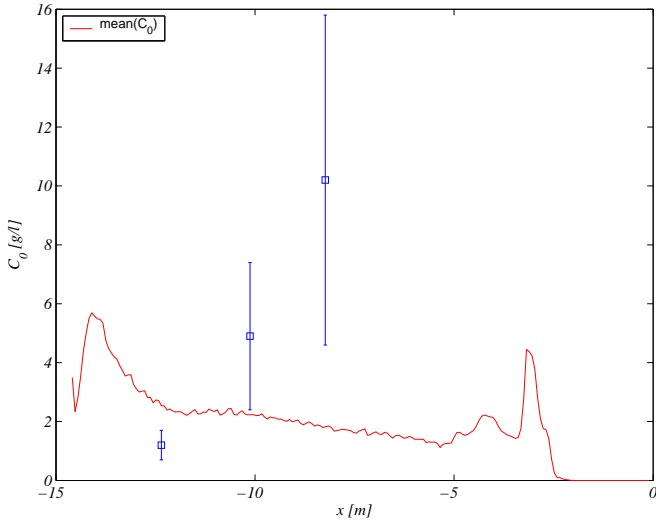


Figure 7: Measured and predicted near-bed concentration over the surf zone without breaking generated turbulence.

then, that the stress-based reference concentration is also relatively constant over the domain, in disparity with the measured concentration data shown in Figure 2. Alternatively, the time-averaged near-bed concentration deriving from both surface breaking turbulence and bed shear is depicted in Figure 8. The relative importance of the two sources of turbulence depends, of course, on empirical parameters such as the length scale and the coefficient of friction, and the results shown in Figure 8 use standard parameters ($l_d = .1h$, $c_f = 0.01$, $e = 0.01$). In the outer surf the suspension due to breaking and friction are similar in magnitude. In the mid and inner surf zone, however, the proximity of the breaking process to the bed makes the breaking-generated dissipation the primary agent of suspension. The simple model accounting for the breaking process demonstrates markedly better agreement with the measured concentration data when compared to the

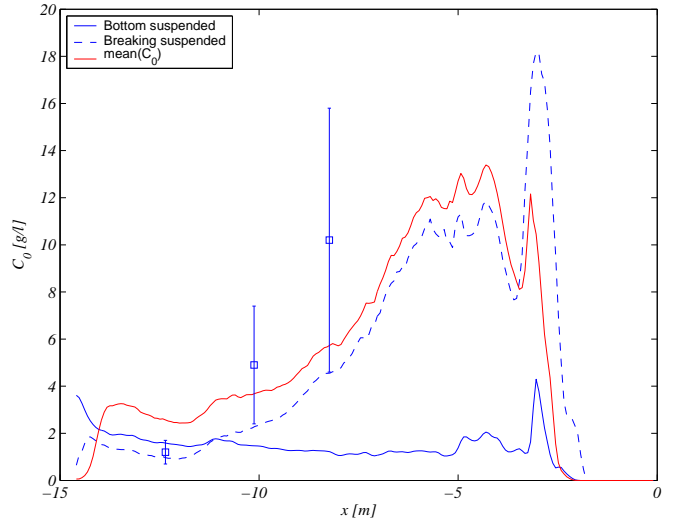


Figure 8: Measured and predicted near-bed concentration over the surf zone accounting for bed shear stress and breaking-generated turbulence

bed stress-based model.

5 Conclusions

Phase-averaged empirical morphology models can provide reasonable predictions when site-specific parameters are available, and the mode is applied within a calibrated range. The results from more general time-averaged processes-based models have been less satisfactory. This deficiency should be expected after considering that steady models don't include the relevant physical processes for entrainment of sediment. Indeed, to correctly predict concentration in a physically-based manner, the time-dependent hydrodynamics need to be suitably modeled. Adopting this viewpoint, the Boussinesq equations were used to model hydrodynamics from a saturated surf zone. The bulk energy loss from the

hydrodynamic solution provided a surface breaking production mechanism for a simple turbulence balance. Production owing to the bottom boundary layer was predicted with a simple conceptual model, and suspension rates are directly determined from a combined dissipation. Reference concentration models that are based on only bottom shear compare poorly with the measurements. Improved results are presented for the simple entrainment model that includes the effect of both bottom shear and breaking turbulence that reaches the bed.

The Chief of Engineers, US Army Corps of Engineers, is acknowledged for granting permission to publish this work.

- Bradshaw, P. 1974. "Effect of free-stream turbulence on turbulent shear layers." *I.C. Aero Report 74-10*. Dept. of Aeronautics, Imperial College of Science and Technology, London.
- Cox, D.T., N. Kobayashi, and A. Okayasu, "Experimental and numerical modeling of surf zone hydrodynamics." *Res. Rept. CACR-95-07*, Ctr. for Applied Coastal Res., Univ. of Delaware, Newark, DE, 1995.
- Dingemans, M. W., 1997 *Water Wave Propagation over Uneven Bottoms*. World Sci. River Edge, NJ, (1997).
- Fredsoe, J., and R. Deigaard. 1992. *Mechanics of Coastal Sediment Transport*, World Sci., River Edge, NJ.
- George, R.A., R.E. Flick, and R.T. Guza. 1994. "Observations of turbulence in the surf zone." *J. Geophys. Res.*, 99(C1), 801–810.
- Hamilton, D.G., B.A. Ebersole, E.R. Smith, and P. Wang. 2000. "Development of a large-scale laboratory facility for sediment transport research." *Technical Report, ERDC/CHL TR-01-22*, Vicksburg, MS.
- Hunt, J.C.R. 1984. "Turbulence structure in thermal convection and shear-free boundary layers." *J. Fluid Mech.* Vol. 138, pp. 161-184.
- Johnson, B.D. and J. Smith. 2006. "Observations of sand transport in the surf zone." *Proceedings of the 30th Coastal Engineering Conference*, ASCE, 2485–2497.
- Kobayashi, N., and B.D. Johnson. 2001. "Sand suspension, storage, advection and settling in surf and swash zones." *J. Geophys. Res.* 106(C5) 9363–9376.
- Madsen, P.A., and O.R. Sorensen. 1992. "A new form of the Boussinesq equations with improved linear dispersion characteristics. Part 2. A slowly-varying bathymetry." *Coast. Eng.*, 18, 183–204.
- Musumeci, R.E., I.A. Svendsen, J. Veeramony. 2005. "The flow in the surf zone: a fully nonlinear Boussinesq-type of approach." *Coast. Eng.* 52: 565–598.
- Nielsen, P., 1992. *Coastal Bottom Boundary Layers and Sediment Transport*. World Sci., River Edge, NJ.
- Okayasu, A., 1989. "Characteristics of turbulence structures and undertow in the surf zone." PhD Thesis, Yokohama Nat. U., 1989
- Raubenheimer, B., R.T. Guza, S. Elgar, and N. Kobayashi. 1995. "Swash on a gently sloping beach." *J. Geophys. Res.*, 100(C5), 8751–8760.
- Svendsen, I.A. 2006. *Introduction to nearshore hydrodynamics* World Sci., River Edge, NJ.
- Van Rijn, L.C. 1984. "Sediment pickup functions." *J. of Hydraulic Engineering*, 110, 10, 1494–1502.